Computational Materials Science 51 (2011) 194–205

Contents lists available at SciVerse ScienceDirect

Computational Materials Science

journal homepage: www.elsevier.com/locate/commatsci

Theoretical prediction of the structural, electronic and optical properties of SnB_2O_4 (B = Mg, Zn, Cd)

D. Allali [a], A. Bouhemadou [a,b,*], S. Bin-Omran [b]

[a] Laboratory for Developing New Materials and their Characterization, Department of Physics, Faculty of Science, University of Setif, 19000 Setif, Algeria
[b] Department of Physics and Astronomy, College of Science, King Saud University, P.O. Box 2455, Riyadh 11451, Saudi Arabia

ARTICLE INFO

Article history:
Received 6 June 2011
Received in revised form 13 July 2011
Accepted 24 July 2011
Available online 28 August 2011

Keywords:
A. Spinels
B. Ab initio calculations
D. Structural properties
D. Electronic structures
D. Optical properties
D. Pressure effect

ABSTRACT

The structural, electronic and optical properties of the cubic spinels SnB_2O_4, with B = Mg, Zn and Cd, were studied by means of the full-potential (linear) augmented plane wave plus local orbitals method within the local density and generalized gradient approximations for the exchange-correlation potential. The Engel–Vosko form of the generalized gradient approximation (EV-GGA), which better optimizes the potential for the band structures, was also used. The results of bulk properties, including lattice constants, internal parameters, bulk moduli and their pressure derivatives are in good agreement with the literature data. The band structures show a direct band gap (Γ–Γ) for the three compounds. The computed band gaps using the EV-GGA show a significant improvement over the more common GGA. All the calculated band gaps increase with increasing pressure and fit well to a quadratic function. Analysis of the density of states revealed that the lowering of the direct gap (Γ–Γ) from $SnMg_2O_4$ to $SnZn_2O_4$ to $SnCd_2O_4$ can be attributed to the *p–d* mixing in the upper valence band of $SnZn_2O_4$ and $SnCd_2O_4$. We present calculations of the frequency-dependent complex dielectric function $\varepsilon(\omega)$. We find that the values of zero-frequency limit $\varepsilon_1(0)$ increase with decreasing the energy band gap. The origin of the peaks and structures in the optical spectra is determined in terms of the calculated energy band structures.

1. Introduction

The spinels are crystalline solids well known to mineralogists, chemists and solid-state physicists. The most abundant spinel groups, of stoichiometry AB_2X_4, are those formed by some metals in oxidation states II–III (II = Cd, Mg, Mn, Zn; III = Al, Ga, In) and II–IV (IV = Si, Ge, Sn). X usually stands for oxygen or one chalcogen [1]. Many of these compounds are semiconductors. In the last few decades, there has been an increasing interest in understanding of the physical and chemical properties of the cubic-spinel family, in particular, since $MgAl_2O_4$ became a technologically important compound [2,3]. Spinel compounds have been subject of many experimental and theoretical works, focusing on the structural [4–6], electronic [7–9], mechanical [5,6,10–13] and optical properties [14–17]. They are characterized by a several desirable properties, e.g. a high melting point, high reflectivity, high strength, chemical resistively at elevated temperatures and low electrical loss [17,18] which make them candidate materials for numerous applications in geophysics, magnetism, catalysis and environment [19–23].

The recent growing demand for high-performance and low-cost transparent conducting oxides (TCO) in optoelectronic devices such as flat-panel displays, windshield defrosters and solar cells [24,25] has led to an extensive search for new TCO materials with higher transparency and conductivity [26]. Among many binary and ternary oxides, the oxide spinels: $SnMg_2O_4$, $SnZn_2O_4$ and $SnCd_2O_4$ have emerged as promising TCO's. These materials have been the subject of numerous experimental and theoretical investigations [4,26–33]. Experimentally, these three compounds have been synthesized using many elaboration methods, such as thermal evaporation, high temperature calcinations, sol–gel synthesis, ball-milling and rf magnetron sputtering [34,31]. These materials usually exist in either cubic spinel structure or and orthorhombic structure, according to the growth conditions [31,32,26]. Theoretically, Segev and Wei [26], studying the cation distribution in spinel oxides including $SnZn_2O_4$ and $SnCd_2O_4$, proved that $SnZn_2O_4$ is stable in the cubic inverse spinel structure and $SnCd_2O_4$ is stable in the orthorhombic structure. More recently, Garcia and co-workers [33], performed a theoretical study on the pressure-induced phase transitions in $SnZn_2O_4$. They proved that this compound is stable in the cubic inverse spinel structure.

First-principles calculations offer one of the most powerful tools for carrying out theoretical studies of an important number of

* Corresponding author at: Laboratory for Developing New Materials and their Characterization, Department of Physics, Faculty of Science, University of Setif, 19000 Setif, Algeria. Tel.: +21 336925128; fax: +21 336925101.
E-mail addresses: a_bouhemadou@yahoo.fr, abouhemadou.v@ksu.edu.sa (A. Bouhemadou).

0927-0256/$ - see front matter © 2011 Elsevier B.V. All rights reserved.
doi:10.1016/j.commatsci.2011.07.046

physical and chemical properties of the condensed matter. It is now possible to explain and predict properties of solids which were previously inaccessible to experiments. We therefore think that it is worthwhile to perform a systematic first-principles study on the trends of the structural, band structure, total density of states, charge carrier effective mass, dielectric function, reflectivity, refractive index and loss function for the family of the cubic normal spinel oxides SnB_2O_4 depending on the type of B element (B are Mg, Zn and Cd) using the full-potential (linear) augmented plane wave plus local orbitals (FP-APW + lo) method in order to provide reference data for the experimentalists and to complete existing theoretical work on this fascinating class of materials.

The paper is divided in three parts. In Section 2, we briefly describe the computational techniques used in this study. The most relevant results obtained for the structural, electronic and optical properties for the $SnMg_2O_4$, $SnZn_2O_4$ and $SnCd_2O_4$ compounds are presented and discussed in Section 3. Finally, in Section 4 we summarize the main conclusions of our work.

2. Computational method

The first-principles calculations are performed by employing full-potential (linear) augmented plane wave plus local orbitals (FP-(L)APW + lo) approach [34–36] based on the density functional theory (DFT) [37,38] and implemented in the Wien2k package [39]. The exchange-correlation potential for structural properties was calculated using the generalized gradient approximation based on Perdew et al. (PBE-GGA) [40], while for electronic properties in addition to that, the Engel–Vosko scheme (EV-GGA) [41] was applied. In the FP-(L)APW + lo method, the unit cell is divided into non-overlapping spheres centered at atomic sites (muffin-tin spheres) of radius R_{MT} and an interstitial region. In the muffin-tin spheres, the Kohn–Sham wave functions are expanded in a linear combination of radial functions time spherical harmonics, and in the remaining space of the unit cell a plane wave basis set is chosen. The basis set inside each muffin-tin sphere is split into core and valence subsets. The core states are treated within the spherical part of the potential only and are assumed to have a spherically symmetric charge density totally confined inside the muffin-tin spheres. The valence part is treated within a potential expanded into spherical harmonics. The valence wave functions inside the spheres are expanded up to $l_{max} = 10$. The Sn ($4p^6 4d^{10} 5s^2 5p^2$), Mg ($2p^6 3s^2$), Zn ($3p^6 3d^{10} 4s^2$), Cd ($4p^6 4d^{10} 5s^2$) and O ($2s^2 2p^6$) states are treated as valence electrons. The R_{MT} values are taken to be 2.2, 1.6, 1.9, 2.2 and 1.2 atomic units (*a.u.*) for Sn, Mg, Zn, Cd and O, respectively. A plane wave cut-off $K_{max} = 4(a.u.)^{-1}$ is chosen for the expansion of the wave functions in the interstitial region. The k integrations over the Brillouin zone (BZ) are performed up to $6 \times 6 \times 6$ Monkorst–Pack (16 k-points in the irreducible Brillouin zone (IBZ)) [42]. The self-consistent calculations are considered to be converged when the total energy of the system is stable within 10^{-5} Ry.

3. Results and discussion

3.1. Structural properties

Cubic normal spinels with chemical formula AB_2X_4 have a closed-packed face-centred-cubic structure, with space group *Fd-3m* (#227), and its unit cell contains eight AB_2X_4 unit formulas ($A_8B_{16}X_{32}$). The 32 anions (X^{-2} anions) occupy the 32e site. The cations occupy either the tetrahedral 8*a* site (A^{+4} cations) or the octahedral 16*d* (B^{+2} cations). There is only one internal parameter u, which specifies the deviation of the anions in the ⟨1 1 1⟩ direction. The description of the atomic positions in spinels dependent on the choice of setting for the origin in the *Fd-3m* space group. Two different equipoints with point symmetries $-43m$ and $-3m$ are possible choices for the unit cell origin. In the ideal spinel with no anion deviation, $u_{ideal} = 0.25$ or 0.375 for origins at $-3m$ or $-43m$ symmetry, respectively [43]. The thirty two X atoms are positioned at the (u, u, u) positions, the eight A atoms at $(0.125, 0.125, 0.125)$ and the sixteen B atoms at $(0.5, 0.5, 0.5)$. Then its crystal structure is characterized by two free parameters: the lattice constant a and the internal anion parameter u. In most spinels, u lies between 0.24 and 0.275, if the origin of the unit cell is taken at $-3m$ point symmetry. The unit cell of the cubic spinel $SnZn_2O_4$ is depicted in Fig. 1 as a prototype for the cubic normal spinel family.

We have performed a full optimization of all the free parameters of the space group, the unit cell volume and the coordinate of the oxygen atom (u). More specifically, we first searched for a minimum of the total energy with respect to the volume. Keeping the latter constant, we then searched for a minimum of the total energy by varying u. The whole process was then iterated until the total energy was minimized with respect to the two parameters simultaneously. The total energies versus lattice parameters are fitted to the Murnaghan's equation of state (EOS) [44] to determine the ground state properties such as the equilibrium lattice constant a_0, the bulk modulus B_0 and the bulk modulus pressure derivative B'. The calculated structural parameters (a_0, B_0 and B') of $SnMg_2O_4$, $SnZn_2O_4$ and $SnCd_2O_4$ at zero pressure are summarized in Table 1. A detailed comparison is made with the available experimental data and the previous calculations. There is good agreement between our results and the available theoretical and experimental data; the predicted values of a_0 differ from the experimental ones by not more than 1.7%. As it can be seen from the data, the a_0 values of the series SnB_2O_4 phases increase in the following sequence: a_0 ($SnMg_2O_4$) < a_0 ($SnZn_2O4$) < a_0 ($SnCd_2O_4$), meanwhile the B_0 values decreases in the following sequence: B_0 ($SnMg_2O_4$) > B_0 ($SnZn_2O_4$) > B_0 ($SnCd_2O_4$), i.e. in inverse sequence to a_0 – in agreement with the well-known relationship between B_0 and the lattice constants: $B_0 \propto V_0^{-1}$, where V_0 is the unit cell volume. The internal parameter u decreases in going from $SnMg_2O_4$ to $SnZn_2O_4$ to $SnCd_2O_4$.

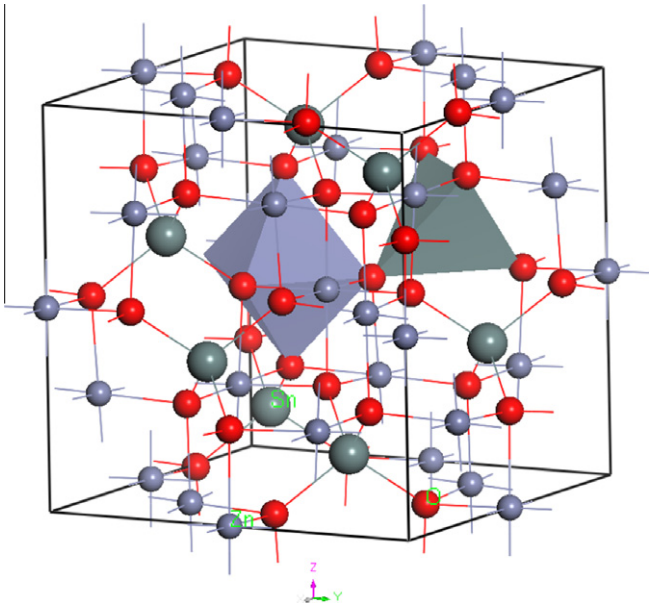

Fig. 1. A schematic representation of the cubic spinel structure of $SnZn_2O_4$. Oxygen atoms (red spheres) occupy the corners of the octahedral and tetrahedral; Sn and Zn are at the centres of the tetrahedral and octahedral, respectively. (For color interpretation mentioned in this figure legend the reader is referred to see the web version of this article.)

Table 1
Calculated lattice constant a_0, internal structure parameters u, bulk modulus B_0 and its pressure derivative B' for the $SnMg_2O_4$, $SnZn_2O_4$ and $SnCd_2O_4$ compounds, compared with experimental data and previous theoretical calculations.

	$SnMg_2O_4$			$SnZn_2O_4$			$SnCd_2O_4$		
	Present	Exp	Others	Present	Exp	Others	Present	Exp	Others
a_0	8.709[A]	8.600[a]	8.566[a]	8.785[A]	8.6574[a]		8.6310[a]	9.335[A]	9.143[a]
	8.557[B]	8.639[b]	8.777[c]	8.569[B]	8.650[d]	8.5500[e]	9.112[B]	9.151[f]	9.120[e]
	8.635[g]	8.525[c]			8.610[h]	8.688[i]		9.177[k]	
								9.174[k]	
u	0.2557[A]	0.2500[a]	0.2583[a]	0.2555[A]	0.2650[a]	0.2580[a]	0.2502[A]	0.2670[a]	0.2510[a]
	0.2569[B]	0.2600[b]	0.2582[c]	0.2574[B]	0.2650[d]	0.2580[e]	0.2491[B]	0.2580[f]	0.2500[e]
	0.2600[g]	0.2569[c]			0.2650[h]			0.2556[k]	
								0.2559[k]	
B_0	151.48[A]		135.49[c]	150.95[A]	168.9[j]	193.4[i]	124.19[A]		
	182.92[B]		162.66[c]	191.78[B]		185.6[j]	161.87[B]		
B'	4.881[A]		4.31[c]	4.700[A]	4.0[j]	4.0[i]	4.551[A]		
	4.893[B]		4.43[c]	4.948[B]		4.0[j]	4.998[B]		

[A] GGA.
[B] LDA.
[a] Ref. [4].
[b] Ref. [46].
[c] Ref. [47].
[d] Ref. [48].
[e] Ref. [26].
[f] Ref. [49].
[g] Ref. [50].
[h] Ref. [51].
[i] Ref. [33].
[j] Ref. [33] (cubic inverse spinel structure).
[k] Ref. [52].

3.2. Electronic properties

Now we discuss our results pertaining to the electronic properties of $SnMg_2O_4$, $SnZn_2O_4$ and $SnCd_2O_4$ via the energy bands, density of states and effective mass. It is well known that the LDA and the GGA usually underestimate the energy gap [53,54]. This is mainly due to the fact that they have simple forms that are not sufficiently flexible for accurately reproducing both exchange-correlation energy and its charge derivative. Engel and Vosko, by considering this shortcoming, constructed a new functional form of the GGA which has been designed to give better exchange correlation potential at the expense of less agreement as regards exchange energy. This approach, which is called the EV-GGA [42], yields a better band splitting and some other properties which mainly depend on the accuracy of the exchange-correlation potential. On the other hand, in this method, the quantities which depend on an accurate description of the exchange energy such as the equilibrium volumes and bulk modulus are in poor agreement with experiment. The calculated band structure profiles using the PBE-GGA and the EV-GGA for $SnMg_2O_4$, $SnZn_2O_4$ and $SnCd_2O_4$ were similar except for the value of their band gaps which are higher within EV-GGA. The energy bands of $SnMg_2O_4$, $SnZn_2O_4$ and $SnCd_2O_4$ along the high symmetry directions in BZ at the equilibrium lattice parameters within the EV-GGA are given in Fig. 2. Both the top of the valence band (VBM) and the bottom of the conduction band (CBM) are located at Γ point for the three studied compounds, making the three compounds to be a direct gap material. The calculated values of band gaps for the three compounds studied herein are given in Table 2, along with other theoretical results available in the literature. Our calculated direct energy band gap (Γ–Γ) using the PBE-GGA compare favorably with those obtained earlier using the same functional [26,44]. However, it is

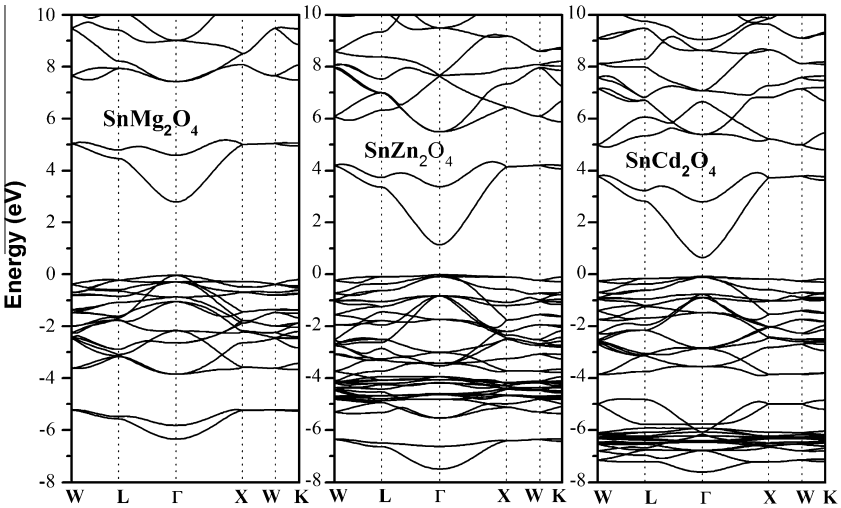

Fig. 2. Electronic band structure for the cubic spinel $SnMg_2O_4$, $SnZn_2O_4$ and $SnCd_2O_4$. The Fermi level is set to zero.

Table 2
Calculated first- and second-order pressure derivatives of some indirect (K–Γ, L–Γ) and direct (Γ–Γ, L–L, X–X, K–K, W–W) band gaps for $SnMg_2O_4$, $SnZn_2O_4$ and $SnCd_2O_4$. $E_g(p) = E_g(0) + \alpha p + (\beta/2)p^2$, $E_g(0)$, the gap at zero pressure, is in eV, α is in 10^{-2} eV $(GPa)^{-1}$, β is in 10^{-4} eV $(GPa)^{-2}$.

	K–Γ	L–Γ	Γ–Γ	L–L	X–X	K–K	W–W
$SnMg_2O_4$							
Present							
$E_g(0)$(LDA)	4.473	3.963	2.086	4.201	4.841	4.706	5.020
$E_g(0)$(GGA)	4.468	3.927	2.019	4.132	4.775	4.643	4.940
$E_g(0)$(GGA-EV)	4.986	4.499	2.823	4.691	5.284	5.151	5.418
Others[49]			2.470[a]				
			1.850[a]				
α	5.42	5.06	4.54	4.740	5.40	5.08	5.31
β	−5.64	−4.72	−4.22	−3.30	−4.29	3.58	−3.65
$SnZn_2O_4$							
Present							
$E_g(0)$(LDA)	3.592	2.844	0.542	2.953	3.822	3.709	4.008
$E_g(0)$(GGA)	3.633	2.863	0.439	2.948	3.813	3.723	4.020
$E_g(0)$(GGA-EV)	4.075	3.374	1.155	3.450	4.242	4.156	4.424
Others [31]			0.500[b]				
α	3.59	3.17	1.90	3.36	3.89	3.90	3.92
β	−2.86	−2.47	−1.17	−2.78	−3.23	−3.45	−3.15
$SnCd_2O_4$							
Present							
$E_g(0)$(LDA)	3.717	2.708	0.230	2.792	3.876	3.796	4.139
$E_g(0)$(GGA)	3.284	2.380	0.008	2.465	3.492	3.387	3.654
$E_g(0)$(GGA-EV)	3.713	2.909	0.735	2.984	3.903	3.805	4.038
Others [31]			0.170[b]				
α	4.22	3.47	2.97	3.44	3.99	4.09	3.97
β	−3.32	−2.13	−1.82	−1.83	−2.27	−2.94	−1.56

[a] Ref. [50].
[b] Ref. [26].

clear from Table 2 that our calculated band gap values using the EV-GGA show a significant improvement over the other exchange-correlation functional. No experimental data on these oxides are available for comparison with the predicted values.

To further elucidate the nature of the electronic band structure, we have calculated the total and atomic site projected densities of states (TDOS and PDOS, respectively) of these compounds. The origin of energy is at the Fermi level. The main bands, in the energy range between −8 and 6 eV, of interest for the interpretation of optical spectra are shown in Fig. 3. In $SnMg_2O_4$, the upper valence bands (between −4.8 and 0 eV) are composed mostly of O-2*p* states with small contributions from Mg-3*s* + 2*p* and Sn-5*p*. The replacement of Mg with Zn (then with Cd) in $SnZn_2O_4$ ($SnCd_2O_4$) brings the contributions from Zn-3*d* (Cd-4*d*) electrons to the upper valence band in $SnZn_2O_4$ ($SnCd_2O_4$). Instead of the O-2*p*-dominated band in the $SnMg_2O_4$, the zinc 3*d* band and the cadmium 4*d* appear inside the upper valence band of $SnZn_2O_4$ and $SnCd_2O_4$, respectively, which hybridize strongly with the oxygen *p* states. Due to the difference in the electronegativity between the comprising elements, some ionic character can be expected. The bonding character may be described as a mixture of covalent-ionic. A new structure originating from Zn-3*d* and Cd-4*d* appears in the DOS spectre of $SnZn_2O_4$ (between −7.4 and −6.2 eV) and $SnCd_2O_4$ (between −7.7 and −4.6 eV), respectively. It is therefore expected that changes in the electronic properties of $SnZn_2O_4$ ($SnCd_2O_4$) as compared to those of $SnMg_2O_4$ would solely be due to the mixing of the Zn-3*d* (Cd-4*d*) and O-2*p* orbitals. In the three compounds, the bottom of the conduction band is predominantly composed of Sn-*p* states.

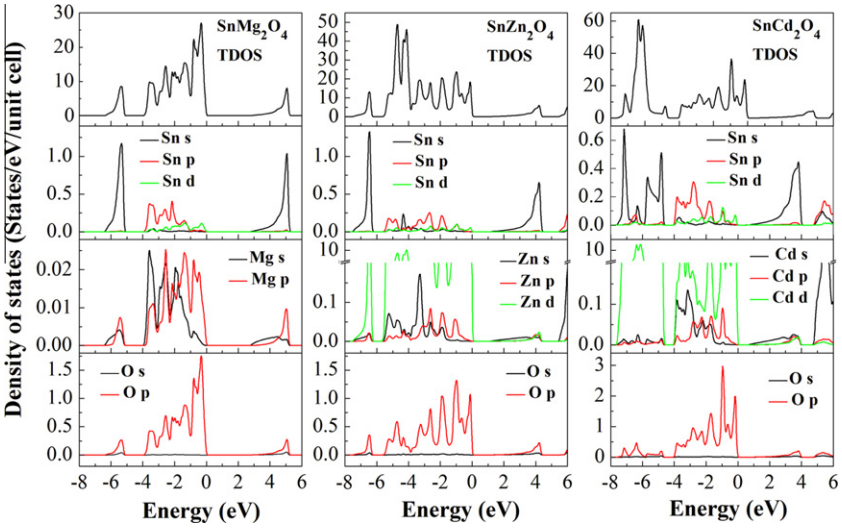

Fig. 3. Site and angular momentum decomposed DOS for the cubic spinel $SnMg_2O_4$, $SnZn_2O_4$ and $SnCd_2O_4$. The Fermi level is set to zero.

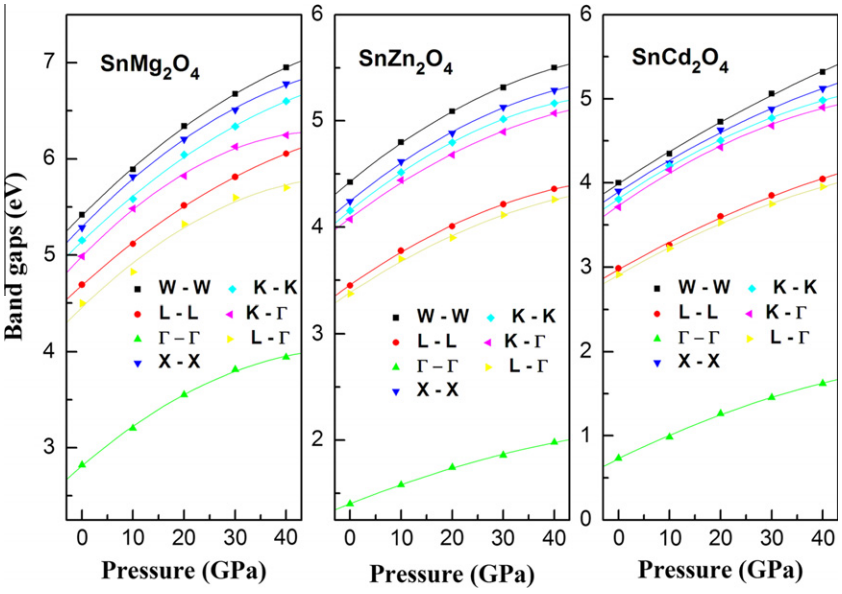

Fig. 4. Pressure dependence of direct (Γ–Γ, L–L, X–X, K–K, W–W) and indirect (K–Γ, L–Γ) energy band gaps for the cubic spinel $SnMg_2O_4$, $SnZn_2O_4$ and $SnCd_2O_4$. The solid lines represent the quadratic fit function.

Table 3
Calculated effective masses of the electron (m_e^*), the heavy hole (m_{hh}^*) and the light hole (m_{lh}^*) (in units of free electron mass m_0) for the $SnMg_2O_4$, $SnZn_2O_4$ and $SnCd_2O_4$ compounds, using GGA-EV method, compared with previous results.

	$SnMg_2O_4$	$SnZn_2O_4$		$SnCd_2O_4$	
		Present	Other [26]	Present	Other [26]
m_e^*/m_0 (Γ–X)	0.35	0.23	0.188[a]	0.20	0.141
m_e^*/m_0 (Γ–L)	0.37	0.25		0.22	–
m_{hh}^*/m_0 (Γ–X)	2.62	14.87		32.44	–
m_{hh}^*/m_0 (Γ–L)	6.83	2.82		2.40	–
m_{lh}^*/m_0 (Γ–X)	0.46	1.44		1.11	–
m_{lh}^*/m_0 (Γ–L)	0.39	1.24		0.68	–

Generally, lowering of the band gap is expected with the substitution of the heavier cations (e.g. Zn for Mg and Cd for Zn) in a series of compounds which are structurally isomorphous [55]. The calculated results in fact show a lowering of the calculated results show a lowering of the gap in the following sequence: $E_g(SnMg_2O_4) > E_g(SnZn_2O_4) > E_g(SnCd_2O_4)$ (Table 2). The role of *d* states in defining the electronic properties of the II–VI semiconductors [56], zinc aluminate [4], zinc aluminate, zinc galate [55] and cubic spinels AB_2O_4, where A = Si and Ge, and B = Mg, Zn and Cd [57,58] has been discussed. It has been reported that the *p*–*d* hybridization at Γ repels the valence band maximum upwards without affecting the conduction band minimum. Hence the lowering of the calculated direct gap Γ–Γ from 2.823 eV in $SnMg_2O_4$ (EV-GGA result) to 1.155 eV in $SnZn_2O_4$ and to 0.735 eV in $SnCd_2O_4$ can be attributed to the presence of the 3*d* and 4*d* states in $SnZn_2O_4$ and $SnCd_2O_4$, respectively.

In order to investigate the effects of the pressure on the size of the energy gaps of $SnMg_2O_4$, $SnZn_2O_4$ and $SnCd_2O_4$, the band energies at selected symmetry points are studied as a function of

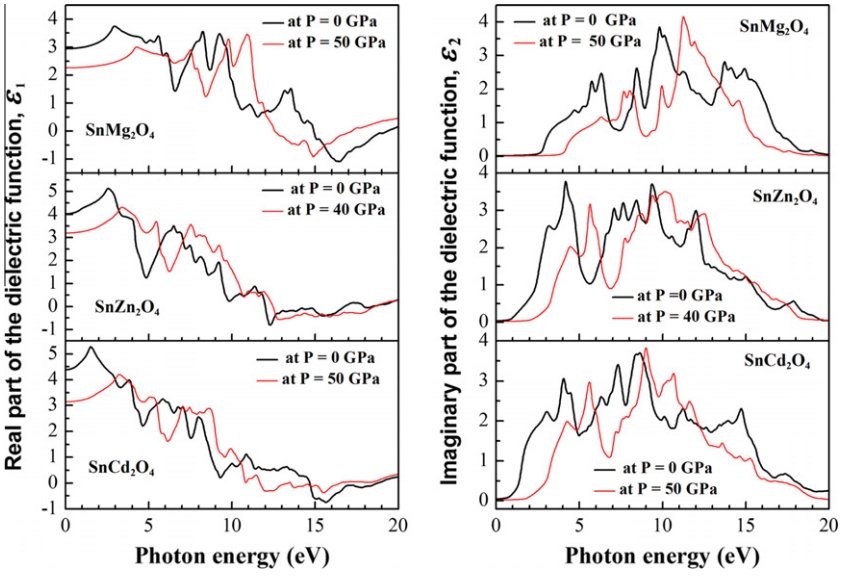

Fig. 5. Calculated real and imaginary parts of the dielectric function for the spinel cubic $SnMg_2O_4$, $SnZn_2O_4$ and $SnCd_2O_4$ at zero pressure and at 50 GPa.

Table 4
Calculated static dielectric constant $\varepsilon(0)$, static refractive index $n(0)$, first energy for which dispersion is null $\{E(n=1)\}$ and pressure coefficient of refractive index $n(0)$ of $SnMg_2O_4$, $SnZn_2O_4$ and $SnCd_2O_4$. Energy values are in eV, $\varepsilon_1(0)$ and $n(0)$ are dimensionless.

Systems	$\varepsilon_1(0)$	$n(0)$	$E(n=1)$	$\frac{1}{n_0}\frac{dn}{dp}(10^{-5}(\mathrm{GPa})^{-1})$
$SnMg_2O_4$	2.990	1.720	15.13	−3.889
$SnZn_2O_4$	4.042	2.020	12.19	−4.170
$SnCd_2O_4$	4.382	2.090	14.77	−4.240

pressure. Fig. 4 shows the plots of the variation with pressure of the direct gaps (Γ–Γ, L–L, X–X, K–K, W–W) and indirect gaps (K–Γ, L–Γ) for $SnMg_2O_4$, $SnZn_2O_4$ and $SnCd_2O_4$. All the calculated band gaps are well fitted to a quadratic function: $E_g(p) = E_g(0) + \alpha p + (\beta/2)p^2$, where E_g is the band gap energy, p is the pressure, α and β are the first- and second-order pressure dependences, respectively. The calculated values of α and β of the mentioned gaps are given in Table 2. All the gaps increase when the pressure is enhanced.

The effective charge-carrier mass m^* have been evaluated by fitting the valence band (conduction band) to a parabola according to $E = \frac{\hbar^2 k^2}{2m^*}$, where m^* denotes the charge-carrier effective mass, in a very small range close to the VBM and CBM in order to guarantee parabolicity. The evaluated effective charge-carrier masses at the Γ point from the band dispersions of the VBM and CBM towards X and L directions in the Brillouin zone are summarized in Table 3 for the three studied materials. The effective electron mass is indicated by the under script "e" (m_e^*) and the hole mass by "h" (m_h). In the $SnMg_2O_4$, $SnZn_2O_4$ and $SnCd_2O_4$ cubic spinels, the valence-band maximum is flat, representing the rather large effective mass for the holes. On the other hand, calculation show that the electron effective mass is smaller in $SnCd_2O_4$ than that $SnZn_2O_4$ and is much smaller than that $SnMg_2O_4$ (Table 3). Thus our calculations predict a higher mobility of electrons in $SnCd_2O_4$ relative to both $SnMg_2O_4$ and $SnZn_2O_4$. The effective mass values in the Γ → X and Γ → L directions in the BZ are different, indicating its anisotropy. Note that our calculated electron effective mass values are slightly larger than those reported by Ref. [26].

3.3. Optical properties

The dielectric function of an anisotropic material is a complex symmetric tensor. In the limit of the linear optics, in the case of non-spin polarization, and within the independent particle approximation, random phase approximation, the imaginary part of the dielectric tensor can be computed from knowledge of the electronic band structure of a solid from the well-known relation [44,59]:

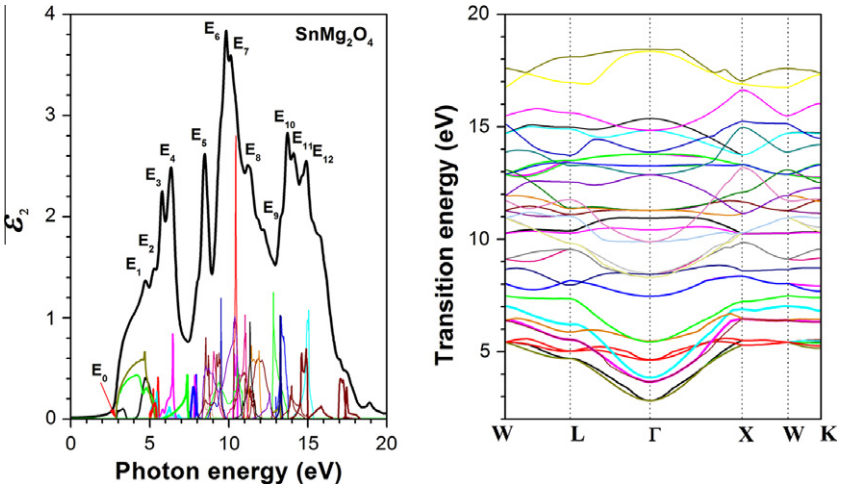

Fig. 6. The decomposition of the imaginary part of the dielectric function into band-to-band contributions (left panel) and the transition energy band structure (right panel) for $SnMg_2O_4$.

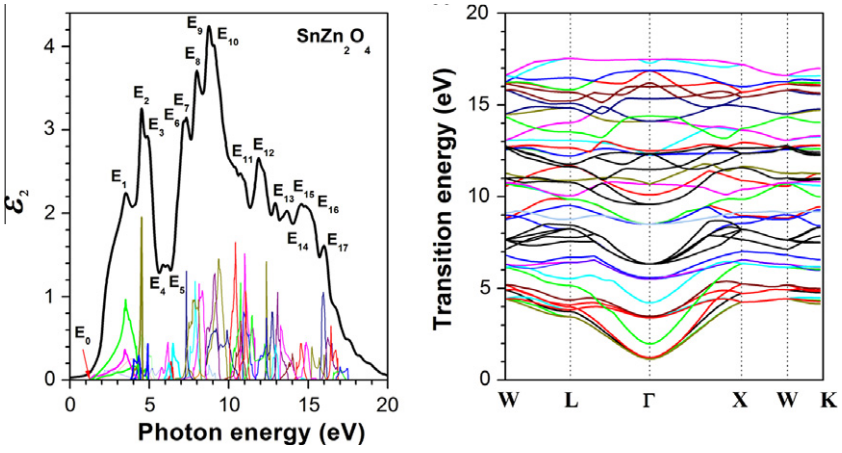

Fig. 7. As Fig. 6, but for $SnZn_2O_4$.

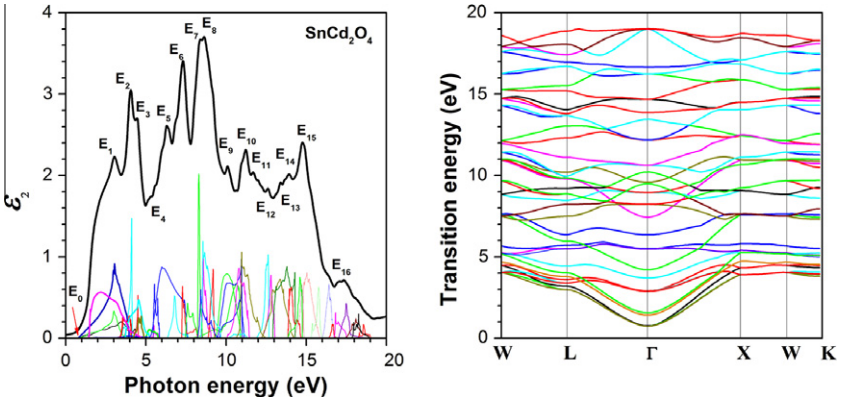

Fig. 8. As Fig. 6, but for $SnCd_2O_4$.

Table 5
Optical transitions in $SnMg_2O_4$. The energies are in eV.

Structure	Peak position	Transitions	Energy
E_0	2.82	(V_1–C_1) Γ–Γ	2.82
		(V_2–C_1) Γ–Γ	
		(V_3–C_1) Γ–Γ	
E_1	4.73	(V_1–C_1) L–Γ–X	4.69
		(V_2–C_1) Γ–X	4.78
		(V_3–C_1) L–Γ–X	4.66
E_2	5.28	(V_1–C_1) W–L, Γ–X, W–K	5.40
		(V_1–C_2) W–L,Γ–X	5.22
		(V_2–C_2) Γ–X, W–K	5.44
		(V_3–C_2) W–L, Γ–X–W–K	5.32
E_3	5.78	(V_1–C_2) W–L, Γ–X	5.52
		(V_2–C_2) W, Γ–X, W	5.43
E_4	6.35	(V_5–C_1) W–L, Γ–X	6.24
		(V_6–C_1) W–L, Γ–X, W–K	6.46
E_5	8.47	(V_1–C_3) L–Γ–X	7.94
		(V_2-C_3) W–L–Γ–X	7.86
		(V_3–C_3) W–L–Γ–X, W–K	7.77
E_6	9.83	(V_{13}–C_4) W–L–Γ–X–W–K	9.51
		(V_{13}–C_5) L–Γ–X	9.36
		(V_{14}–C_4) W–L–Γ–X–W–K	9.23,9.36,9.45
E_7	10.12	(V_8–C_2) W–L–Γ–X	10.44
		(V_9–C_2) W–L–Γ–X	10.35, 10.51
		(V_{12}–C_4) W–L, Γ–X, W–K	10.94
		(V_{13}–C_5) W–L, X–W–K	10.54, 10.63
		(V_{14}–C_5) W–L, X–W–K	10.38
E_8	11.20	(V_{10}–C_3) W–L–Γ–X–W–K	11.03, 11.22, 11.31
		(V_{10}–C_4) W–L–Γ–X–W–K	11.30, 11.43, 11.57
		(V_{12}–C_4) W–L, Γ–X	11.00
		(V_{12}–C_5) W–L–Γ, X–W	11.43, 11.55
		(V_{14}–C_6) W–L–Γ, W–K	11.03, 11.08
		(V_{14}–C_7) W–L–Γ–X	10.90, 11.36
E_9	12.20	(V_8–C_3) W–L, X–W–K	12.83
		(V_{10}–C_5) W–L, Γ–X	11.88, 12.11
		(V_{12}–C_5) W–L, X–W–K	11.90
		(V_{12}–C_6) W–L–Γ–X, W–K	12.12, 12.45, 12.60
E_{10}	13.71	(V_8–C_4) W–L–Γ–X	13.33, 13.48, 13.50
		(V_9–C_3) W–L–Γ–X–W	13.25
		(V_9–C_4) W–L–Γ–X–W–K	13.27
		(V_{11}–C_8) W–L, Γ–X–W–K	13.98
		(V_{11}–C_9) W–L, Γ–X–W–K	13.89
E_{11}	14.60	(V_9–C_6) L–Γ–X–W	14.61
E_{12}	14.90	(V_8–C_6) W–L–Γ–X	14.96, 15, 15.06
		(V_9–C_6) W–L–Γ	14.89, 14.94

Table 6
Optical transitions in $SnZn_2O_4$. Energies are in eV.

Structure	Peak position	Transitions	Energy
E_0	1.20	(V_1–C_1) Γ–Γ	1.20
		(V_2–C_1) Γ–Γ	
		(V_3–C_1) Γ–Γ	
E_1	3.50	(V_2–C_1) W–L, Γ–X	3.45
		(V_3–C_1) W–L, Γ–X	3.48
E_2	4.52	(V_1–C_1) W–L, Γ–X–W	4.74
		(V_1–C_2) W–L, Γ–X	4.36, 4.29
		(V_2–C_2) W–L, W–K	4.47
		(V_3–C_2) W–L, Γ–X–W–K	4.34
		(V_5–C_2) W–L, Γ–X	4.50, 4.59
E_3	4.87	(V_1–C_1) W–L, X–W	4.74
		(V_1–C_2) W–L, X–W–K	4.92
		(V_5–C_1) W–L, Γ–X, W–K	5.00
		(V_5–C_2) W–L, Γ–X 4.94,	5.03
E_4	5.86	(V_4–C_2) W–L, Γ–X	5.76
E_5	6.15	(V_1–C_3) W–L–Γ–X	6.37
		(V_2–C_3) W–L–Γ–X–W	6.50
		(V_4–C_2) W–L, Γ–X–W–K	6.09, 6.15, 6.17
E_6	7.17	(V_{10}–C_4) W–L–Γ–X–W–K	7.45
		(V_{13}–C_3)W–L–Γ–X	7.33
		(V_{13}–C_4) L–Γ–X	7.47
E_7	7.33	(V_{10}–C_4) W–L–Γ–X–W–K	7.45, 7.60
		(V_{12}–C_3) W–L–Γ–X, W–K	7.58
		(V_{13}–C_3) W–L–Γ–X	7.33
		(V_{13}–C_4) W–L–Γ–X–W–K	7.62, 7.74, 7.83
E_8	7.99	(V_{10}–C_4) W–L–Γ	8.18
		(V_{10}–C_5) L–Γ–X	8.18
		(V_{12}–C_3) L–Γ–X–W	7.87
		(V_{12}–C_4) W–L–Γ–X–W–K	8.14, 8.23, 8.34
		(V_{13}–C_4) W–L–Γ–X–W–K	8.09
E_9	8.76	(V_8–C_5) L–Γ–X	8.69
		(V_{10}–C_5) W–L, X–W–K	8.93
		(V_{10}–C_7) W–L–Γ–X	8.56, 8.60, 8.66, 8.75
E_{10}	9.06	(V_8–C_4) W–L–Γ–X, W–K	9.37, 9.42
		(V_8–C_5) W–L–Γ–X–W	9.20, 9.89
		(V_9–C_4) W–L–Γ–X–W–K	8.86, 9.09, 9.12
		(V_{10}–C_7) W–L, Γ–X–W–K	9.07, 9.14
E_{11}	10.75	(V_6–C_4) W–L–Γ–X–W–K	10.24, 10.72, 11
		(V_9–C_7) W–L–Γ–X–W	10.24, 10.35, 10.42
		(V_9–C_8) W–L–Γ–X–W	10.09, 10.35, 10.60, 10.74
		(V_9–C_9) W–L–Γ–X	10.94
		(V_{11}–C_{11}) L–Γ–X 10.46,	10,76
		(V_{11}–C_{12}) W–L, Γ–X–W–K	10.90, 11,05
E_{12}	11.88	(V_6–C_4) W–L–Γ	11.05, 11.64
		(V_9–C_9) W–L, Γ–X–W–K	11.26, 11.44
		(V_{11}–C_{13}) W–L–Γ–X–W–K	11.45, 12.25
		(V_{11}–C_{14}) W–L–Γ–X	12.00, 12.06
E_{13}	12.95	(V_6–C_7) W–L–Γ–X–W–K	12.36, 12.58
		(V_6–C_8) W–L–Γ–X–W–K	12.30, 12.41, 12.70
		(V_6–C_9) W–L–Γ–X–W–K	12.99, 13.07
		(V_9–C_{12}) W–L–Γ–X–W–K	12.80, 12.93
		(V_{11}–C_{14}) W–L–Γ–X–W–K	12.37
		(V_{11}–C_{15}) W–L–Γ–X, W–K	12.49
E_{14}	13.65	(V_6–C_9) Γ–X–W–K	13.22, 13.50
		(V_6–C_{10}) W–L, Γ–X	13.81, 13.99
		(V_9–C_{13}) L–Γ–X	13.27
E_{15}	14.58	(V_6–C_{11}) W–L–Γ–X–W–K	14.27, 14.52
E_{16}	14.80	(V_6–C_{12}) W–L–Γ–X–W–K	14.66, 14.80, 14.87
		(V_6–C_{13}) L–Γ	15.23
		(V_7–C_{13}) W–L, X–W–K	14.60
E_{17}	16.00	(V_6–C_{13}) W–L–Γ–X–W–K	15.70, 16
		(V_6–C_{14}) W–L–Γ–X–W	15.94
		(V_6–C_{15}) W–L–Γ–X–W–K	16,22, 16,44, 16.50
		(V_6–C_{16}) W–L–Γ–X–W–K	16.43, 16.72
		(V_6–C_{17}) W–L, X–W	16.60, 16,70
		(V_7–C_{14}) W–L–Γ–X–W	15.26, 15.43

Table 7
Optical transitions in $SnCd_2O_4$. Energies are in eV.

Structure	Peak position	Transitions	Energy (eV)
E_0	0.77	(V_1–C_1) Γ– Γ	0.77
		(V_2–C_1) Γ– Γ	
		(V_3–C_1) Γ– Γ	
E_1	3.04	(V_1–C_1) W–L, Γ–X	3.44
		(V_2–C_1) W–L, Γ–X	3.004
		(V_3–C_1) W–L–Γ–X	2.97, 3.04
E_2	4.05	(V_1–C_1) W–L, Γ–X	4.30
		(V_1–C_2) W–L, Γ–X	3.80
		(V_2–C_2) W–L, Γ–X, W–K	4.09
		(V_3–C_2) W–L, Γ–X–W–K	3.98
E_3	4.45	(V_1–C_1) W–L, Γ–X	4.30
		(V_1–C_2) Γ–X–W–K	4.50
		(V_2–C_2) W–L, Γ–X	4.11
		(V_4–C_2) W–L–Γ–X	4.54
		(V_5–C_2) W–L, Γ–X	4.56, 4.70
E_4	5.55	(V_1–C_3) W–L–Γ–X, W–K	5.53, 5.72
E_5	6.30	(V_8–C_1) W–L–Γ–X	5.99
		(V_8–C_2) W–L–Γ–X	6.77, 6.81
E_6	7.31	(V_8–C_1) W–L, Γ–X, W–K	7.40
		(V_8–C_2) W–L, Γ–X–W–K	7.60
		(V_9–C_3) W–L, Γ–X, W–K	7.28, 7.36
		(V_9–C_4) W–L, Γ–X–W–K	7.60, 7.78
E_7	8.40	(V_8–C_3) W–L–Γ–X–W–K	8.56, 8.71, 8.98
		(V_9–C_3) L–Γ–X	8.13
		(V_9–C_4) W–L–Γ–X, W–K	8.30
		7.91,	
		(V_9–C_5) L–Γ–X	8.42
		(V_9–C_6) L–Γ	8.55
E_8	8.62	(V_8–C_4) W–L–Γ–X–W–K	9.05, 9.18
		(V_9–C_3) L–Γ–X	8.21
		(V_9–C_5) W–L–Γ–X	8.77, 8.94
		(V_9–C_6) W–L–Γ–X	8.65, 8.83
E_9	10.09	(V_7–C_1) W–L, Γ–X, W–K	10.66, 10.74, 10.81
		(V_7–C_2) W–L, Γ–X–W–K	10.85, 10.94
		(V_8–C_5) W–L, Γ–X	10.05
		(V_8–C_6) W–L–Γ–X	10.06
		(V_8–C_7) W–L–Γ–X	10.46, 10.08
		(V_8–C_9) L–Γ–X	10.97
E_{10}	11.22	(V_8–C_6) W–L, X–W	10.95
		(V_8–C_7) W–L, Γ–X	11.10
		(V_8–C_8) W–L, Γ–X–W	10.80, 10.94, 11.08, 11.18
		(V_8–C_9) W–L–Γ–X	10.97, 11.11
E_{11}	11.67	(V_8–C_8) W–L, X–W	11.35
		(V_8–C_9) W–L, Γ–X	11.34, 11.50
E_{12}	12.62	(V_7–C_3) L–Γ–X	12.45, 12.52, 12.62
		(V_7–C_4) W–L–Γ–X	12.80, 12.99
		(V_7–C_5) L–Γ–X	12.91
		(V_8–C_9) Γ–X–W	12.30
E_{13}	13.41	(V_7–C_5) W–L–Γ–X	13.35, 13.57
		(V_7–C_6) L–Γ–X	13.12
E_{14}	13.94	(V_7–C_6) W–L, Γ–X	13.80
		(V_7–C_7) W–L–Γ–X	13.86, 13.90, 13.94
E_{15}	14.76	(V_6–C_8) W–L–Γ, X–W–K	14.71, 14.74
		(V_6–C_9) W–L–Γ–X–W–K	14.86, 14.93, 15.18, 15.27
		(V_6–C_{10}) W–L–Γ–X–W–K	15.38, 15.54, 15.77
		(V_7–C_6) W–L, X–W	14.25, 14.29
		(V_7–C_7) W–L, X–W–K	14.47, 14.53, 14.58
E_{16}	17.34	(V_6–C_{11}) W–L–Γ–X–W	16.61
		(V_6–C_{12}) W–L–Γ–X–W	16.62, 16.68
		(V_6–C_{13}) W–L–Γ–X	16.80, 16.98
		(V_6–C_{14}) W–L–Γ–X–W–K	17.49
		(V_6–C_{15}) W–L–Γ, X–W–K	17.89, 18.09
		(V_6–C_{16}) W–L–Γ–X–W–K	17.95, 18.26
		(V_6–C_{17}) W–L, W–K	18.31

$$\mathrm{Im}\varepsilon_{\alpha\beta}(\omega) = \varepsilon_2^{\alpha\beta}(\omega) = \frac{4\pi e^2}{m^2\omega^2} \times \sum_{if} \int \langle f|p^{\alpha}|i\rangle\langle i|p^{\beta}|f\rangle W_i(1-W_f)(E_f - E_i - \hbar\omega)d^3k.$$

In this expression, $\langle f|p_\alpha|i\rangle$ and $\langle f|p_\beta|i\rangle$ are the dipole matrix elements corresponding to the α and β directions of the crystal (x, y or z), and f, i are the final and initial states, respectively. W_n is the Fermi distribution function for the nth state, and E_n is the electron energy in the nth state. The real part of the frequency-dependent dielectric function expression $\varepsilon_{\alpha\beta}(\omega)$ is computed from $\varepsilon_2^{\alpha\beta}(\omega)$ using the Kramers–kronig relations in the form

$$\varepsilon_1^{\alpha\beta}(\omega) = \delta_{\alpha\beta} + \frac{2}{\pi}P\int_0^{\infty}\frac{\omega'\varepsilon_2^{\alpha\beta}(\omega')}{\omega'^2-\omega^2}d\omega',$$

where P is the Cauchy principal value of the integral. Optical constants, such as the refractive index $n(\omega)$, the extinction coefficient $k(\omega)$, the reflectivity $R(\omega)$, the coefficient of absorption $\alpha(\omega)$ and the loss function $L(\omega)$, can be calculated from the dielectric function $\varepsilon(\omega) = \varepsilon_1(\omega) + i\varepsilon_2(\omega)$ using the well known relations. For the cubic structure, the optical properties are isotropic, i.e. there is only one independent component (ε_{xx}).

Calculation of the optical properties requires a dense mesh of energy eigenvalues and the corresponding eigenvectors, so one needs to use a dense mesh of uniformly distributed k-points to calculate the optical constants. Since ε_2 is usually calculated first, we chose it as a reference for the assessment of convergence. The 16 k-points calculation did not converge, while the 120 and 165 k-points in the irreducible part of the BZ calculations coincide. Thus, we assumed convergence at 120 k-points and this is the number of k-points we used for the calculation of the optical properties. The imaginary part of the dielectric function ε_2, and the coefficient extinction k and reflectivity R, represent different ways to assess how the electromagnetic energy is taken when interacting with a material medium. Two closely related optical parameters indicate how electromagnetic energy is dispersed when it penetrates in a medium: the real part of the complex dielectric function ε_1 and the real part of the complex refraction index n. In order to perform comprehensive study of this important aspect of the optical properties of the $SnMg_2O_4$, $SnZn_2O_4$ and $SnCd_2O_4$ compounds, we have computed and studied these optical parameters.

The real and imaginary parts of the frequency-dependent dielectric function for the dielectric function for the cubic spinels $SnMg_2O_4$, $SnZn_2O_4$ and $SnCd_2O_4$ are shown in Fig. 5. The static dielectric constant $\varepsilon_1(0)$ is given by the low energy limit of $\varepsilon_1(\omega)$. Note that we do not include phonon contributions to the dielectric screening, and $\varepsilon_1(0)$ corresponds to the static optical dielectric constant ε_∞. The calculated static dielectric constants $\varepsilon_1(0)$ for the studied materials are listed in Table 4. We find that e values of $\varepsilon_1(0)$ increases with decreasing energy gap. This could be explained on the basis of the Penn model [60,61]. Penn model is based on the expression $\varepsilon_1(0) \approx 1 + (\hbar\omega_p/E_g)^2$. It is clear that $\varepsilon_1(0)$ is inversely proportional with E_g. Hence smaller E_g yields larger $\varepsilon_1(0)$. We can determine E_g from his expression by using the value of $\varepsilon_1(0)$ and the plasma energy $\hbar\omega_p$.

It would be useful to identify the transitions that are responsible for the spectral structures in the optical spectra. The determination of the origins of the different peaks and features of the optical spectra are performed on the basis of decomposing each spectrum to its individual pair contribution, i.e., contribution from each pair of valence v_i and conduction c_j bands ($v_i - c_j$), and plotting the transition (from valence to conduction) band structures, i.e., transition energy $E(k) = E_{cj}(k) - E_{vi}(k)$ (right panels in Figs. 6–8). These techniques allow the knowledge of the bands which contribute more to the peaks and their locations in the Brillouin zone [see Ref. [62] and references cited therein]. The main contributions to the optical spectra originate from the top valence bands to the lower conduction bands. E_0 is the edge of optical absorption. This point is the $\Gamma_v - \Gamma_c$ splitting which gives the threshold for direct optical transition between the highest valence band and the lowest conduction band. This is known as the fundamental absorption edge. This critical point is followed by some structures centered at E_i points. The positions of the main E_i peaks and the corresponding interband transition and their locations in the Brillouin zone are reported in Tables 5–7 When these materials are compressed, the positions of all critical points cited above are shifted with an enhanced energy comparative to that at zero pressure. The reason lies on the enhancement of direct gaps under pressure effect. Although their positions are shifted under pressure, these points still have the same type as that at zero pressure. Fig. 9 shows the calculated results for the pressure dependence of the static dielectric constant $\varepsilon_1(0)$ for SnMg2O4, SnZn2O4 and SnCd2O4. As it can be seen from Fig. 9, the decrease of the dielectric constants with pressure is parabolic in both compounds.

The refractive index and the extinction coefficient are displayed in Fig. 10. The static refractive index $n(0)$ values for $SnMg_2O_4$, $SnZn_2O_4$ and $SnCd_2O_4$ and energy for which dispersion is null

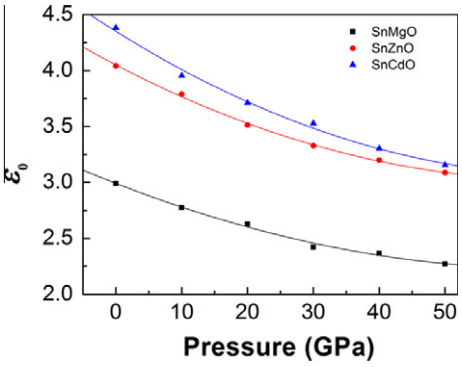

Fig. 9. Pressure dependence of the static dielectric constants $\varepsilon(0)$ for the cubic spinel $SnMg_2O_4$, $SnZn_2O_4$ and $SnCd_2O_4$.

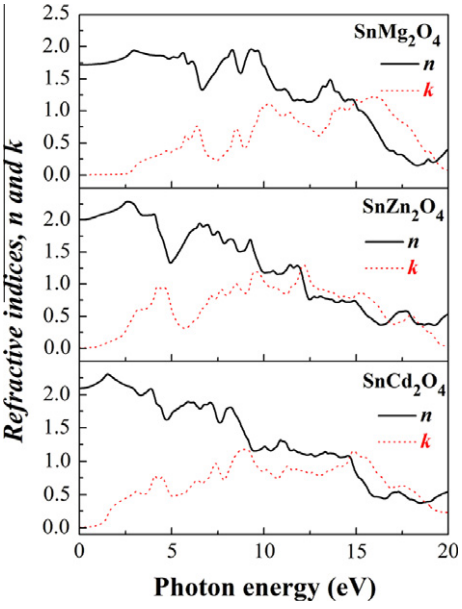

Fig. 10. Refractive index $n(\omega)$ and extinction coefficient $k(\omega)$ spectra for the cubic spinel $SnMg_2O_4$, $SnZn_2O_4$ and $SnCd_2O_4$.

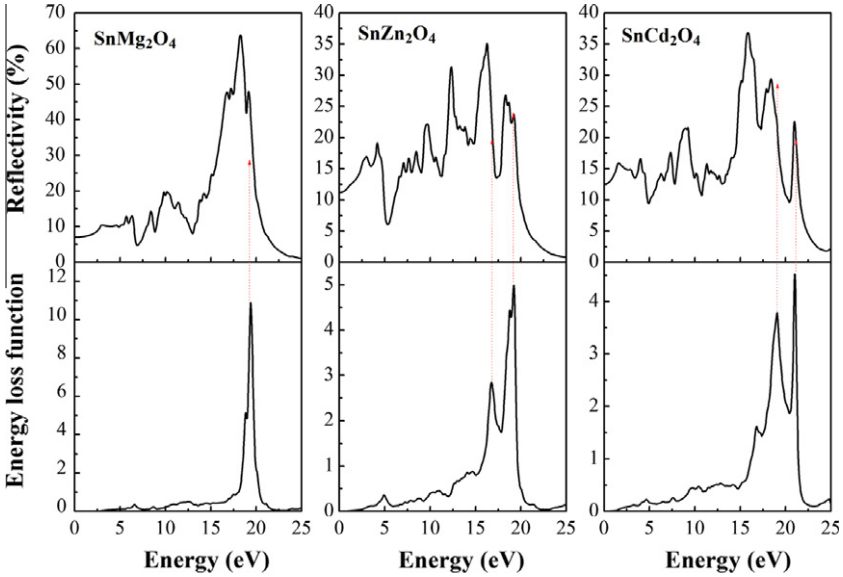

Fig. 11. Optical reflectivity $R(\omega)$ and electron energy-loss function $L(\omega)$ spectra for the cubic spinel $SnMg_2O_4$, $SnZn_2O_4$ and $SnCd_2O_4$.

$E(n = 1)$ are extracted in Table 4. The origin of the structures in the imaginary part of the dielectric function also explains the structures in the refractive index. The pressure derivative of the static refractive index $n(0)$ of these compounds is determined by a linear fit and the results are listed in Table 4. From this table, we can notice that the increase of pressure leads to the decrease of the refractive index.

In Fig. 11, we show the reflectivity spectrum $R(\omega)$ for the three compounds. The $R(\omega)$ values for the three compounds are not approach to the unity towards zero energy, which means that these compounds behave like semiconductors. Fig. 11 presents also the electron energy loss function $L(\omega)$. $L(\omega)$ is an important factor describing the energy loss of a fast electron traversing in a material. The peaks in $L(\omega)$ spectra represent the characteristic associated with the plasma resonance and the corresponding frequency is the so called plasma frequency ω_p. The peaks of $L(\omega)$ correspond to the trailing edges in the reflection spectra, for instance, the peak of $L(\omega)$ for $SnMg_2O_4$ is at about 19.34 eV corresponding to the abrupt reduction of $R(\omega)$.

4. Conclusions

We have used an ab initio FP-(L)APW + lo method to determine the structural, electronic and optical properties of the cubic spinel $SnMg_2O_4$, $SnZn_2O_4$ and $SnCd_2O_4$. The computed structural parameters are in good agreement with the experimental findings; validating the herein used method. The energy band structure calculations showed that the valence band maximum and conduction band minimum are located at Γ point in the Brillouin zone, resulting in a direct energy band gap in the three studied compounds. Results obtained for energy band gaps using EV-GGA are larger than that within PBE-GGA. The all calculated band gaps increase with increasing pressure and well fit to a quadratic function. The effective charge-carrier masses are estimated from the band structure. Analysis of the DOS revealed that the lowering of the direct gap Γ–Γ from $SnMg_2O_4$ to $SnZn_2O_4$ to $SnCd_2O_4$ can be attributed to the *p–d* mixing in the upper valence band of $SnZn_2O_4$ and $SnCd_2O_4$. The decomposition of the dielectric functions into individual band-to-band contributions and the plotting of the transition band structures allowed identifying the microscopic origin of the features in the optical spectra and the contributions of the different regions in the Brillouin zone. We find that the values of $\varepsilon_1(0)$ increases with decreasing the energy gap. This could be explained on the basis of the Penn model. Refractive index, extinction coefficient, reflectivity and loss function spectra are predicted.

Acknowledgements

The authors extend their appreciation to the Deanship of Scientific Research at King Saud University for funding the work through the research group project No. RGP-VPP-088.

References

[1] P. Garcia Casado, I. Rasines, J. Solid State Chem. 52 (1984) 187.
[2] L. Garcia, A. Beltrán, J. Andrés, R. Franco, J.M. Recio, Phys. Rev. B 66 (2002) 224114.
[3] J. Ruiz-Fuertes, D. Errandonea, F.J. Manjón, D. Martinez-Garcia, A. Segura, V.V. Ursaki, I.M. Tiginyanu, J. App. Phys. 103 (2008).
[4] S.H. Wei, S.B. Zhang, Phys. Rev. B 63 (2001) 045112.
[5] A. Bouhemadou, R. Khenata, Phys. Lett. A 360 (2006) 339.
[6] A. Bouhemadou, R. Khenata, F. Zerarga, Comput. Mat. Sci. 39 (2007) 709.
[7] Mo. Shang-D, W.Y. Ching, Phys. Rev. B 54 (1996) 16555.
[8] R. Khenata, M. Sahnoun, H. Baltache, M.Rérat.Ali.H. Reshak, Y. Al-Douri, B. Bouhafs, Phys. Lett. A 344 (2005) 271.
[9] Y.N. Xu, W.Y. Ching, Phys. Rev. B 43 (1991) 4461.
[10] A. Wanner, Mater. Sci. Eng. A 248 (1998) 35.
[11] A. Martín Pandás, A. Costales, M.A. Blanco, J.M. Recio, V. Luaña, Phys. Rev. B. 62 (2000) 13970.
[12] C. Aksel, B. Rand, F.L. Riley, P.D. Warren, J. Eur. Ceram. Soc. 22 (2002) 745.
[13] P. Thibaudeau, F. Gervais, J. Phys. Condens. Matter 14 (2002) 3543.
[14] A. Ibarra, R. Vila, F.A. Garner, J. Nucl. Mater. 233 (1996) 1336.
[15] I.V. A-Charkin, D.W. Cooke, V.T. Gritsyna, M. Ishimaru, K.E. Sickafus, Vacuum 58 (2000) 2.
[16] T. Suzuki, G.S. Murugan, Y. Ohishi, J. Lumin. 113 (2005) 265.
[17] J.M. Leger, J. Haines, M. Schmidt, J.P. Petit, A.S. Pereira, J.A.H. Jordana, Nature 383 (1996) 401.
[18] W. Jones, L.J. Miles, Proc. Br. Ceram. Soc. 19 (1971) 161.
[19] A. Govindaraj, E. Flahaut, C. Laurent, A. Peigney, A. Rousset, C.N.R. Rao, J. Mater. Res. 14 (1999) 2567.
[20] G. Gusmano, G. Montesperelli, E. Traversa, G. Mattogno, J. Am. Ceram. Soc. 6 (1993) 743.
[21] N.J. Van der Laag, Environmental effects on the fracture of oxide ceramics, Doctorat Thesis, Technical University-Eindhoven, 2002.
[22] T. Irifune, K. Fujino, E. Ohtani, Nature 349 (1991) 409.
[23] R.J. Hill, J.R. Graig, G.V. Gibbs, Phys. Chem. Miner. 4 (1979) 317.
[24] K. Nomura, H. Ohta, T. Ueda, M. Hirano, H. Hosono, Science 300 (2003) 1269.
[25] B.G. Lewis, D.C. Paine, MRS Bull. 25 (2000) 22.
[26] D. Segev, S.H. Wei, Phys. Rev. B 71 (2005) 12529.
[27] T.J. Couts, D.L. Young, X. Li, W.P. Mulligan, X. Wu, J. Vac. Sci. Technol. A 18 (2000) 2646.

[28] X. Wu, T.J. Couts, W.P. Mulligan, J. Vac. Sci. Technol. A 15 (1997) 1057.
[29] B. Li, L. Zeng, F. Zhang, Phys. Status Solidi. A 201 (2004) 960.
[30] D.R. Kammler, T.O. Mason, D.L. Young, T.J. Couts, D. Ko, Poeppelmeier, D.L. Williamson, J. Appl. Phys. 90 (2001) 5979.
[31] M.V. Nikolić, T. Ivetić, D.L. Young, K.M. Paraskevopoulos, T.T. Zobra, V. Blagojević, P.M. Nikolić, D. Vasiljević-Radović, M.M. Ristić, Mater. Sci. Eng. B 138 (2007) 7.
[32] X. Shen, J. Shen, S.J. You, L.X. Yang, L.Y. Tang, Y.C. Li, J. Liu, J. Liu, H. Yang, K. Zhu, Y.L. Liu, W.Y. Zhou, C.Q. Jin, R.C. Yu, S.S. Xie, J. Appl. Phys. 106 (2009) 113523.
[33] L. Gracia, A. Beltrán, J. Andrés, J. Phys. Chem. 115 (2011) 7740.
[34] J.W. Zhao, Li.R. Qin, L.D. Zhang, Solid State Commun. 141 (2007) 663.
[35] G.K.H. Madsen, P. Blaha, K. Schwarz, E. Sjöstedt, L. Nordström, Phys. Rev. B 64 (2001) 195134.
[36] E. Sjöstedt, L. Nordström, D.J. Singh, Solid State Commun. 114 (2000) 15.
[37] K. Schwarz, P. Blaha, G.K.H. Madsen, Comput. Phys. Commun. 147 (2002) 71.
[38] P. Hohenberg, W. Kohn, Phys. Rev. 136 (1964) 86.
[39] W. Kohn, L.J. Sham, Phys. Rev. A 140 (1965) 1133.
[40] P. Blaha, K. Schwarz, G.K.H. Madsen, D. Kvasnicka, J. Luitz, WIEN2k, An Augmented Plane Wave + Local Orbitals Program for Calculating Crystal Properties, Karlheinz Schwarz, Techn. Universität Wien, Austria, 2001.
[41] J.P. Perdew, S. Burke, M. Ernzerhof, Phys. Rev. Lett. 77 (1996) 3865.
[42] E. Engel, S.H. Vosko, Phys. Rev. B 47 (1993) 13164.
[43] H.J. Monkhorst, J.D. Pack, Phys. Rev. B 13 (1976) 5188.
[44] S.M. Hosseini, Phys. Stat. Sol. (b) 245 (2008) 2800.
[46] P. Poix, Ann. Phys. 9 (1964) 261.
[47] M. Reffas, A. Bouhemadou, R. Khenata, T. Ouahrani, S. Binomran, Physica B 405 (2010) 4079.
[48] J. Choisnet, A. Deschanvres, B. Raveau, Comptes Rendus Hebdomadaires des Séances de l'Académie des Sciences, Série C, Sciences Chimiques 266 (1968) 543.
[49] C. Levy-Clément, I. Morgenstern Badarau, Y. Billiet, A. Michel, Comptes Rendus Hebdomadaires des Séances de l'Académie des Sciences, Série C, Sciences Chimiques 270 (1970) 1860.
[50] V.A. Bokov, G.V. Novikov, O.B. Proskuryakov, Y.G. Saksonov, V.A. Rukhtanov, S. Yushchuk, Fizika Tverdogo Tela (Solid State Phys.) 10 (1968) 1080.
[51] T.F.W. Barth, E. Posnjak, Zeitschrift fuer Kristallographie, Kristallgeometrie, Kristallphysik, Kristallchemie 82 (1932) 325.
[52] M.E. Bowden, C.M. Cardile, Powder Diffr. 5 (1990) 36.
[53] P. Dufek, P. Blaha, K. Schwarz K, Phys. Rev. B 50 (1994) 7279.
[54] G.B. Bachelet, N.E. Christensen, Phys. Rev. B 31 (1985) 879.
[55] S.K. Sampath, D.G. Kanhere, R. Pandy, J. Phys. Condens. Matter 11 (1999) 3635.
[56] S.H. Wie, A. Zunger, Phys. Rev. B 37 (1988) 8958.
[57] A. Bouhemadou, R. Khenata, Model., Simul. Mater. Sci. Eng. 15 (2007) 787.
[58] A. Bouhemadou, Model., Simul. Mater. Sci. Eng. 16 (2008) 055007.
[59] A. Ambrosch-Draxl, J.O. Sofo, Comput. Phys. Commun. 175 (2006) 1.
[60] D.R. Penn, Phys. Rev. 128 (1960) 2093.
[61] A.H. Reshak, Z. Charifi, H. Baaziz, Eur. Phys. J. B 60 (2007) 463.
[62] L. Kalarasse, B. Bennecer, F. Kalarasse, J. Phys. Chem. Solids 71 (2010) 314.